Following electroenzymatic hydrogen production by rotating ring disk electrochemistry and mass spectrometry

Jaloliddin Khushvakov,[a†] Robin Nussbaum,[a†] Cécile Cadoux,[a] Jifu Duan,[b] Sven T. Stripp[c] and Ross D. Milton[a*]

[a] Department of Inorganic and Analytical Chemistry, University of Geneva, Sciences II, Quai Ernest-Ansermet 30, 1211 Geneva 4, Switzerland.

[b] Faculty of Biology and Biotechnology, Photobiotechnology, Ruhr-Universität Bochum, Universitätsstrasse 150, 44801 Bochum, Germany.

[c] Department of Physics, Bioinorganic Chemistry, Freie Universität Berlin, 10623 Berlin, Germany.

* Email: ross.milton@unige.ch

† *These authors contributed equally to this work.*

Abstract

Gas-processing metalloenzymes are of interest to new future biotechnologies and bioinspired technologies. Of particular importance are hydrogenases and nitrogenases, which both produce molecular hydrogen (H_2) from proton (H^+) reduction. Here, we report on the use of rotating ring disk electrochemistry (RRDE) and mass spectrometry (MS) to follow the production of H_2 and isotopes produced from deuteron (D^+) reduction (HD and D_2) using a model hydrogen-evolving metalloenzyme [FeFe]-hydrogenase from *Clostridium pasteurianum*. This facilitates enzymology studies independent of non-innocent chemical reductants. We anticipate that these approaches will be of value in resolving the catalytic mechanisms of H_2-producing metalloenzymes and the design of bioinspired catalysts for H_2 production and N_2 fixation.

Keywords

Enzymatic electrochemistry; [FeFe]; Hydrogen; Hydrogenases; Kinetic isotope effect; Metalloenzymes.

Introduction

Due to ever-increasing environmental awareness, there is considerable interest to develop efficient electrocatalysts to produce renewable fuels (such as molecular hydrogen, H_2) or to supplement/delocalize global industrial processes (such as the production of ammonia fertilizer from molecular nitrogen, N_2).[1] Gas-processing metalloenzymes are attractive for new electrochemical biotechnologies and provide inspiration for the design of new catalysts due to desirable catalytic properties such as high selectivity, the use of non-precious and abundant metals in their catalytic cores.[2] Further, their optimal catalytic activities are often found under mild conditions (ambient temperature and pressure, near-neutral pH). Two particular enzymes of interest are hydrogenases and nitrogenases. Hydrogenases are iron- and sulfur-dependent metalloenzymes that are found in all kingdoms of life, which catalyze the reversible reduction of protons ($2H^+$) to H_2 ($E^{0'}$ = −0.414 V *vs*. SHE).[3] Nitrogenases are also iron- and sulfur-dependent metalloenzymes that are found in select archaea and bacteria, which catalyze the fixation of N_2 to NH_3 ($E^{0'}$ = +0.274 V *vs*. SHE),[4] as well as the reduction of H^+ to H_2.[5] The production of one equivalent of H_2 per N_2 reduced is thought to be necessary in order to activate the catalytic cofactor of nitrogenase for N_2 fixation.[6] Thus, there is considerable interest to understand how nitrogenase evolves H_2 for activation as well as how nitrogenase can theoretically divert up to 75% of its electrons toward N_2 fixation over H^+ reduction in aqueous media, a reaction that plagues abiotic N_2–reducing catalytic systems.[6–8]

While hydrogenases and nitrogenases exchange reducing equivalents with small metalloproteins such as ferredoxins or flavodoxins *in vivo*, electrodes have been employed to drive the artificial reduction of H^+ and N_2 by these enzymes *in vitro*.[9–13] Such an approach is attractive not only for new biotechnologies, but also for mechanistic interrogation of their complex catalytic mechanisms where electron transfer to these gas-processing metalloenzymes can be controlled. Here, we demonstrate the use of rotating ring disk electrochemistry (RRDE)

as a technique to follow the production of H_2 from [FeFe]-hydrogenase from *Clostridium pasteurianum* (*Cp*I) wired to a carbon electrode surface within a redox polymer (**Figure 1**). Second, we investigated electroenzymatic hydron reduction by *Cp*I in a 50%/50% H/D buffered electrolyte. We demonstrate the use of online mass spectrometry (MS) to follow H_2, molecular deuterium (D_2) and deuterium hydride (HD) production by an enzyme electrode for the first time, enabling kinetic isotope effect (KIE) studies. These "online" methods provide approaches that can be translated to interrogate other metalloenzymes that produce H_2, as well as characterizing catalytic biases for substrate reduction, *i.e.*, N_2 *vs.* H^+ reduction by nitrogenase.

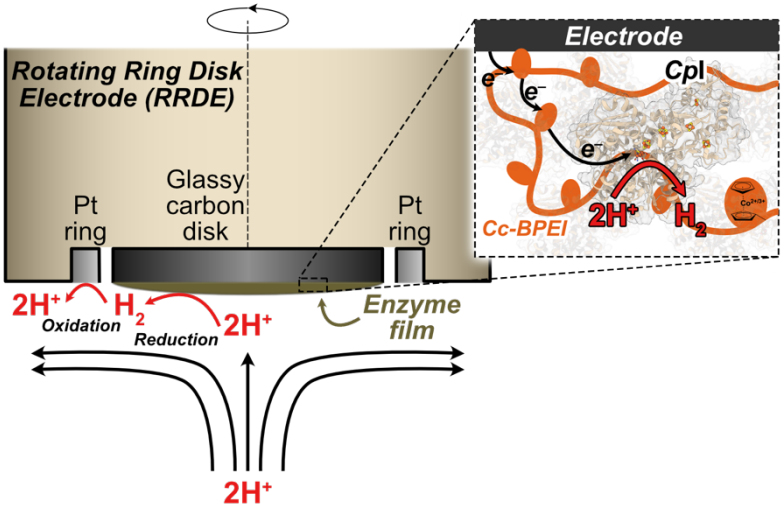

Figure 1. The [FeFe]-hydrogenase from *C. pasteurianum* (*Cp*I) is immobilized within a cobaltocene-containing redox polymer (Cc-BPEI) at the surface of a rotating carbon electrode. The electroenzymatically generated H_2 gas is detected by electrocatalytic oxidation at a rotating Pt ring electrode.

Results

While standard [FeFe]-hydrogenases are particularly active in the H^+ reduction reaction direction,[14] different hydrogenases have previously been reported to undergo H^+ reduction when entrapped within a bis(cyclopentadienyl)cobalt(II)-grafted redox polymer at electrode surfaces.[15] This "cobaltocene" mediator has a reduction potential (E^0) of −0.91 V *vs*. SHE and is well-suited to facilitate electron transfer to hydrogenase for H^+ reduction ($E^{0'}$ = −0.414 V *vs.* SHE).[16] We employed branched poly(ethylenimine)-grafted cobaltocene as the redox polymer (Cc-BPEI)[17] alongside *Cp*I,[18] which can be recombinantly expressed in *Escherichia coli* and activated *in vivo* and *in vitro* (**Figure S1**).[18–21] In the first step, we investigated the activity of *Cp*I and integrity of the "H-cluster" active site cofactor by ATR FTIR spectroscopy. The CO and CN^- ligands of the H-cluster absorb strongly in the frequency regime between 2150 – 1750 cm^{-1} and do not overlap with the absorbance bands of liquid water and protein. Absolute spectra of hydrated sample (0.5 mM *Cp*I or 0.5 mM *Cp*I + 2 mg/mL Cc-BPEI) suggest no degradation of the H-cluster (**Figure S2**). To probe the reactivity of the hydrogenase within the polymer, we recorded ATR FTIR difference spectra triggering the reduction of *Cp*I by changing the atmosphere above the sample from 100% N_2 to 90% N_2 and 10% H_2. **Figure 2a** depicts the decrease of the oxidized state **Hox** (negative bands) over the increase of one-electron reduced states (**Hred´** and **Hred**) and two-electron reduced states (**Hhyd** and **Hsred**). This is the typical behavior of pure [FeFe]-hydrogenase at near-neutral pH (**Figure S3**), as reported earlier.[22–24] Following the reduction and auto-oxidation of *Cp*I in time-resolved experiments further confirms the unperturbed activity of enzyme within the Cc-BPEI polymer

(**Figure 2b** and **Figure S3**). Recent work shows that [FeFe]-hydrogenases can even be reconstituted within redox polymers.[25]

Next, the ability to electrochemically follow H_2 produced by a *Cp*I + Cc-BPEI-functionalized electrode was investigated by rotating ring disk electrochemistry (RRDE). While Pt electrodes efficiently reduce H^+ and oxidize H_2 and RRDE can therefore be employed to follow H_2 production at Pt ring electrodes,[26,27] this technique has not yet been utilized to study mechanisms of H_2-producing metalloenzymes. **Figure 3a** presents a cyclic voltammogram for Cc-mediated H^+ reduction by *Cp*I, where a reductive catalytic "wave" commencing at around <−0.4 V *vs*. SHE was observed representing electroenzymatic H^+ reduction to H_2 at a glassy carbon (GC) disk electrode. A significant H_2 oxidative catalytic "wave" was not observed due to (i) the absence of H_2 in the glovebox (and electrochemical cell) environment, and (ii) the reductive bias imparted by the low reduction potential of the Cc-BPEI redox polymer. Simultaneously, the neighboring Pt ring electrode was poised at a potential sufficiently positive for electrocatalytic H_2 oxidation (*i.e.*, 0 V *vs*. SHE) (**Figure S4**). In order to confirm that the disk reductive currents and the ring oxidative currents

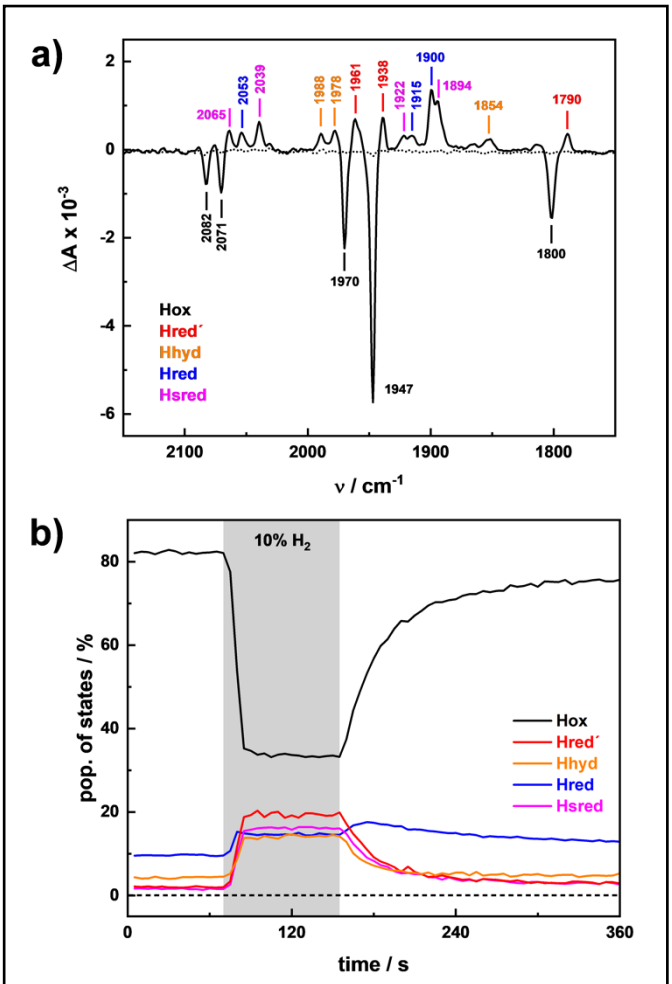

Figure 2. Integrity of the H-cluster and activity of *Cp*I probed by ATR FTIR spectroscopy. **(a)** The figure depicts H_2 – N_2 difference spectra of *Cp*I + 2 mg mL^{-1} Cc-BPEI. Negative bands represent the H-cluster states that prevail under N_2, positive bands are assigned to states accumulated under 10% H_2. The observed pattern is virtually identical to pure *Cp*I. **(b)** Following the time-dependent evolution of states under N_2 and 10% H_2 further confirms the unperturbed activity of *Cp*I within the Cc-BPEI polymer.

did indeed correspond to electroenzymatic H_2 turnover, a control experiment was performed where we exploited the extreme sensitivity of [FeFe]-hydrogenases to O_2.[28] By taking a *Cp*I-modified electrode and deactivating the enzyme by rotating the electrode in an O_2-containing electrolyte solution, the reductive (GC disk) and oxidative (Pt ring) electrocatalytic currents were almost entirely abolished (**Figure S5**).

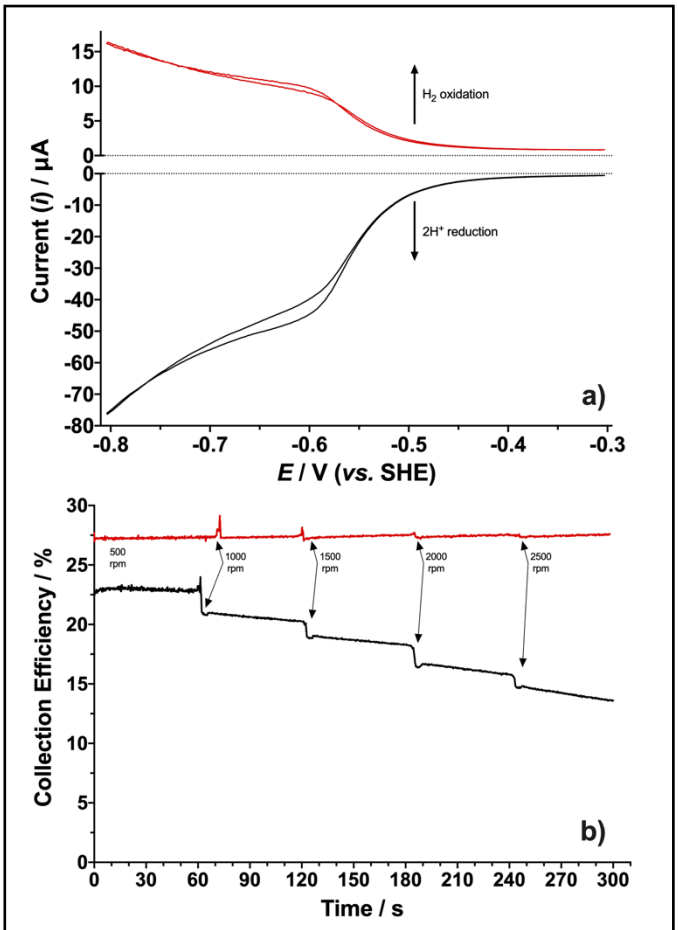

Figure 3. (a) Cyclic voltammogram for electroenzymatic H_2 production (black line) and its subsequent detection by the Pt ring of a RRDE (red line). The scan rate of the *Cp*I-functionalized GC working electrode was 10 mV s^{-1}. The potential of the Pt ring electrode was fixed at 0 V *vs*. SHE during the experiment, although the current is plotted *vs*. the potential applied at the GC electrode. The RRDE was rotated at 1000 rpm in an argon-filled glovebox. Electrolyte = 0.5 M phosphate buffer, pH 6.5. **(b)** A comparison of collection efficiencies obtained for H_2 detection (black line) *vs*. ferricyanide reduction (red line) as a function of rotation rate. Data collected from 2x amperometric *i*-t experiments. For H_2 collection efficiency, the *Cp*I-functionalized disk electrode was poised at −0.8 V and the Pt ring electrode was poised at 0 V *vs*. SHE. Electrolyte = 0.5 M phosphate buffer, pH 6.5. Ferricyanide generation was performed at a disk electrode poised at +0.8 V and ferricyanide reduction was performed at a Pt ring electrode poised at +0.1 V *vs*. SHE. Electrolyte = 0.1 M KCl containing 2 mM

RRDEs have associated collection efficiencies (CEs) corresponding to the quantity of species produced at the disk that is subsequently detected at the ring; this value is specified to be 24.9% for the RRDE used in this study (further information in the Supporting Information). The CE of this setup was first confirmed using the ferrocyanide/ferricyanide couple and found to be around 27% between rotation rates of 500 – 2500 rpm. For the detection of H_2 produced by *Cp*I we observed the CE to reach up to 23% (**Figure 3b, Figure S6 and Figure S7**). Interestingly, the CE was typically found to decrease with increasing rotation rates (**Figure 3b**), which was attributed to

the relatively low solubility of H_2 in aqueous solution and increasingly poor H_2 adsorption at high rotation rates. Further, subsequent electrochemical cleaning of the Pt ring surface (Supporting Information) after performing hydrogenase experiments in phosphate buffer revealed a sharp oxidative peak that disappeared after the first scan (**Figure S8**). We hypothesize that this peak could result from the oxidative stripping of an unknown species that inhibits H_2 adsorption. Further, high phosphate concentrations were found to significantly impact O_2 reduction on Pt electrodes (**Figure S9**), while the CE of the ferrocyanide/ferricyanide couple by RRDE was not significantly impacted.

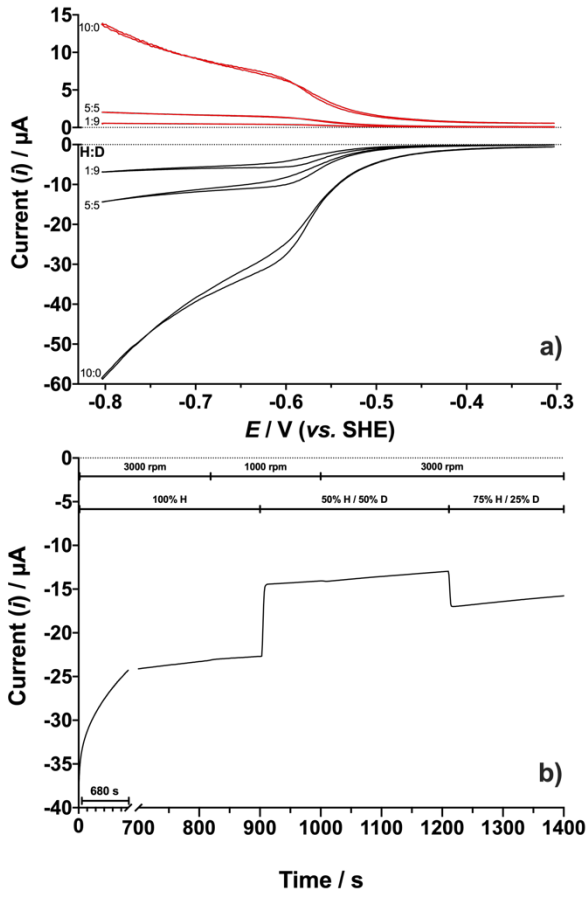

Figure 4. (a) RRDE cyclic voltammograms for electroenzymatic hydron reduction (black line) with varying ratios of H/D, and subsequent product detection (red line). The scan rate of the *Cp*I-functionalized glassy carbon working electrode was 10 mV s^{-1}. The potential of the Pt ring electrode was fixed at 0 V *vs.* SHE during the experiment. The RRDE was rotated at 1000 rpm in an argon-filled glovebox. Electrolyte = 0.5 M phosphate buffer, pH/pD = 6.5. **(b)** Amperometric *i*-t curve demonstrating the sharp decrease in hydron reductive current upon the introduction of 50% D (final) to the electrolyte. Buffer hydron composition and electrode rotation rates are given above the traces. The glassy carbon working electrode was poised at −0.6 V *vs.* SHE. Electrolyte = 0.5 M phosphate buffer, pH/pD = 6.5.

We next evaluated the KIE for hydron reduction by *Cp*I within the Cc-BPEI redox polymer. Initially, the RRDE approach was employed where a significant decrease in the magnitude of the reductive current (diminished H_2 production) was observed in different fractions of D_2O-based electrolyte (**Figure 4a**). In the case where electron transfer to *Cp*I is rate-determining, a change in the electrocatalytic current

(which is proportional to the rate constant) would not be expected and KIE = i_{H_2O}/i_{H_2O} = 1. However, the significant decrease in the rate ($k \propto i$) of hydron reduction indicates that KIE ≠ 1 and we hypothesized that the rate-determining step for hydron reduction could be associated with (i) one or more hydrons, (ii) product release (*i.e.*, $H_2/D_2/HD$)[29] and/or (iii) hydron mass transport (either in the bulk, within the redox polymer film or within *Cp*I). Amperometric *i*-t was subsequently employed to confirm whether bulk mass transport was rate-limiting (**Figure 4b**). We found that the titration of an equivalent D_2O-based phosphate buffer electrolyte (to a final H:D ratio of 1:1) immediately resulted in a decrease in the magnitude of the reductive current by approximately 37%. Increasing the rotation rate of the electrode from 1000 – 3000 rpm did not significantly recover the reductive catalytic current, indicating that bulk mass-transport was not rate-limiting. Further, the subsequent addition of H_2O-based phosphate buffer electrode (with a final H:D ratio of 3:1) resulted in an increase in the magnitude of the reductive current, demonstrating that this effect is reversible.

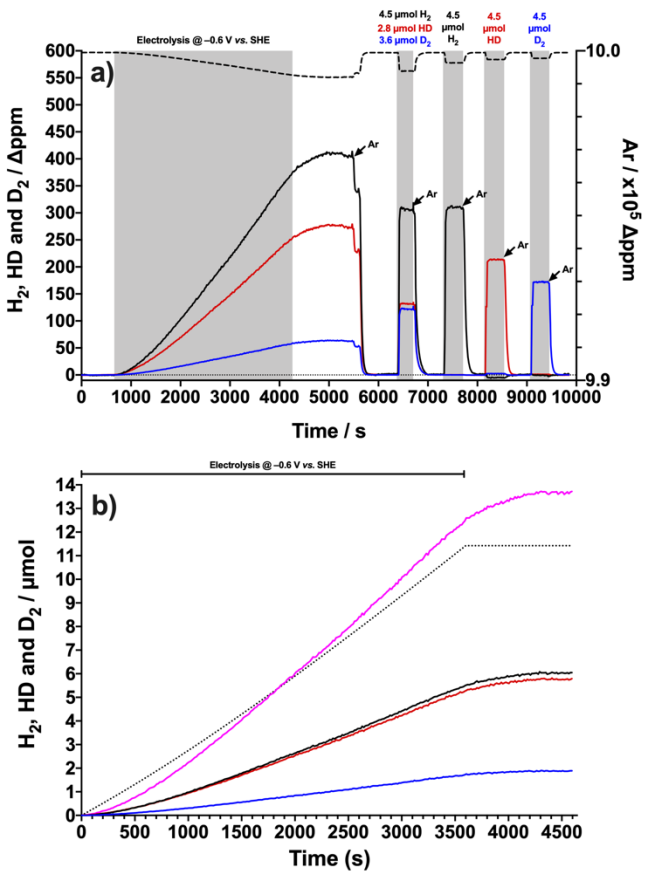

Figure 5. (a) Electrolytic evolution of H_2 (black line), HD (red line) and D_2 (blue line) following the application of −0.6 V *vs.* SHE at a *Cp*I-functionalized carbon paper electrode for 3600 s in 1:1 H:D buffer. Each product was followed simultaneously (in the same run) by mass spectrometry (m/*z* = 2, 3 and 4). Uncalibrated gas quantities are given as baseline corrected changes in ppm. Following electrolysis and in between standard injections, the electrochemical cell was flushed with argon gas (black dashed line) to displace $H_2/HD/D_2$ from the reaction headspace. Electrolyte = 0.5 M phosphate buffer, pH/pD = 6.5. The injection of individual or mixed gas standards demonstrates the differentiation of these products in the same experiment. **(b)** Calibrated quantities of H_2 (black), HD (red), D_2 (blue) and the sum (magenta) produced during 3600 s of bulk electrolysis (from **(a)**). The x-axis was corrected to the start of bulk electrolysis.

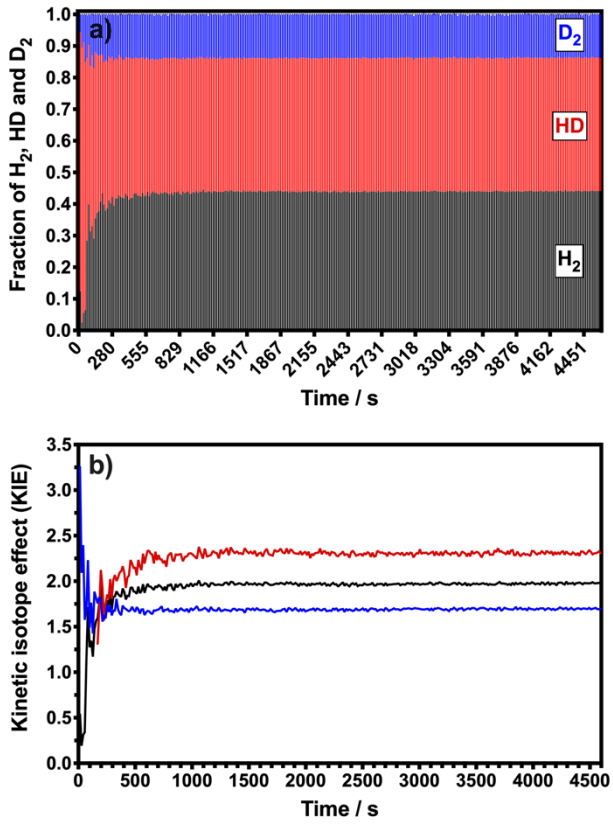

Figure 6. (a) Observed product distribution during electrolysis for 3600 s using a *Cp*I-functionalized carbon paper electrode in 1:1 H:D phosphate buffer, pH 6.5. **(b)** Calculated kinetic isotope effect (KIE) of the *Cp*I-functionalized electrode, based on the observed fraction of each product in (A).

Upon performing electroenzymatic hydron reduction with *Cp*I in a mixed H/D buffer the expected gaseous products would be H_2, D_2 and HD. While we have shown that RRDE is effective in observing the H_2 produced by enzyme electrodes, differentiating between H_2, D_2 and HD at a Pt ring electrode was not expected to be facile. To this end, we utilized an online residual gas analyzer to differentiate between H_2, D_2 and HD. A carbon paper electrode functionalized with *Cp*I and the Cc-BPEI redox polymer was introduced to an electrolyte comprised of 50% deuterated phosphate buffer electrolyte. Bulk electrolysis was performed at −0.6 V *vs.* SHE while simultaneously and continuously following the formation of products (H_2, D_2 and HD) in the headspace of the vial with m/*z* values of 2, 3 and 4 (**Figure 5, Figures S10 and S11**). As demonstrated in **Figure 5a**, it was possible to repeatedly flush the electrochemical cell and make subsequent injections of gas standards for calibration, where H_2, D_2 and HD can either be followed together or individually. After calibration of the cell (**Figure 5b**), the observed product distribution was found to be approximately 0.44:0.42:0.14 for H_2:HD:D_2 at steady-state (**Figure 6a**). Here, we assume that hydrons are sequentially delivered to the H-cluster active site of *Cp*I,[30] arriving at possible pathways for product formation of:

$$\underline{\text{Pathway 1}}:\ [\text{FeFe}] \xrightarrow{+\,\mathbf{H^+}} [\text{FeFe}]_{\text{H}} \xrightarrow{+\,\mathbf{H^+}} [\text{FeFe}] + \ \mathbf{H_2}$$

208 $$\underline{\text{Pathway 2}}:\ [\text{FeFe}] \xrightarrow{+\,\mathbf{H^+}} [\text{FeFe}]_{\text{H}} \xrightarrow{+\,\mathbf{D^+}} [\text{FeFe}] + \ \mathbf{HD}$$

209 $$\underline{\text{Pathway 3}}:\ [\text{FeFe}] \xrightarrow{+\,\mathbf{D^+}} [\text{FeFe}]_{\text{D}} \xrightarrow{+\,\mathbf{H^+}} [\text{FeFe}] + \ \mathbf{HD}$$

210 $$\underline{\text{Pathway 4}}:\ [\text{FeFe}] \xrightarrow{+\,\mathbf{D^+}} [\text{FeFe}]_{\text{D}} \xrightarrow{+\,\mathbf{D^+}} [\text{FeFe}] + \ \mathbf{D_2}$$

211

212 The probabilities (p) of producing H_2, HD (pathways 2 and 3 combined) or D_2 can be
213 then expressed as a function of a KIE and the mole fractions (f_x), as outlined in the Supporting
214 Information.[31] As shown in **Figure 6b**, the KIEs for the overall *Cp*I electrode as calculated for
215 the observed product distribution are ~2 (for H_2), ~2.3 (for HD) and ~1.7 (for D_2). **Figure S11**
216 reports the amperometric *i*-t trace and observed product distribution for a control *Cp*I carbon
217 paper electrode that was prepared under oxic conditions in order to render the enzyme inactive;
218 significantly diminished catalytic currents (x20 fold) and products (x17 fold) were observed,
219 consistent with active *Cp*I being necessary for the observed production of H_2, HD and D_2.

220

221 ## Conclusions

222 We report on the use of RRDE and MS as two different approaches to interrogate H_2 production
223 by gas-processing metalloenzymes at electrode surfaces. The [FeFe]-hydrogenase *Cp*I was
224 used as a "model" metalloenzyme and a cobaltocene-based redox polymer was used to
225 immobilize the enzyme and mediate electrons for H^+ reduction. The Pt ring electrode of an
226 RRDE was shown to be effective at monitoring real-time H_2 production. Further, online MS
227 was employed to follow the production of H_2 and isotopes (HD, D_2) that are produced by
228 hydron reduction at the gas-processing metalloenzyme electrode in a mixed H/D buffer
229 electrolyte. The combination of these techniques will be important to interrogating
230 metalloenzyme mechanisms, notably independent of non-innocent chemical reductants such as
231 dithionite or europium compounds. Future work will seek to identify the origin of the observed

KIE for *Cp*I under these conditions. Moreover, this technique will also be employed to investigate other H_2-producing metalloenzymes for which H^+ reduction is of mechanistic importance, such as nitrogenase.

Acknowledgements

We thank Alexandre Jolly and Darren Martin for assistance with mass spectrometry and enzymatic activity assays. We thank the James Swartz (Stanford University) for sharing the *E. coli* strain used for *Cp*I expression. We thank Thomas Happe for sharing the sample of *Cp*I used for the ATR FTIR experiments. RDM thanks the COMAD of the University of Geneva, the Ernest Boninchi Foundation, the Academic Society of Geneva and the Ernst and Lucie Schmidheiny Foundation for support. STS acknowledges funding by the Deutsche Forschungsgemeinschaft through priority program 1927 (grant agreement 1554/5-1).

References

(1) Holade, Y.; Servat, K.; Tingry, S.; Napporn, T. W.; Remita, H.; Cornu, D.; Kokoh, K. B. Advances in Electrocatalysis for Energy Conversion and Synthesis of Organic Molecules. *ChemPhysChem*, **2017**, *18* (19), 2573–2605.

(2) Jenner, L. P.; Butt, J. N. Electrochemistry of Surface-Confined Enzymes: Inspiration, Insight and Opportunity for Sustainable Biotechnology. *Current Opinion in Electrochemistry*, **2018**, *8*, 81–88.

(3) Lubitz, W.; Ogata, H.; Rüdiger, O.; Reijerse, E. Hydrogenases. *Chem. Rev.*, **2014**, *114* (8), 4081–4148.

(4) Guo, W.; Zhang, K.; Liang, Z.; Zou, R.; Xu, Q. Electrochemical Nitrogen Fixation and Utilization: Theories, Advanced Catalyst Materials and System Design. *Chemical Society Reviews*, **2019**, *48* (24), 5658–5716.

(5) Foster, S. L.; Bakovic, S. I. P.; Duda, R. D.; Maheshwari, S.; Milton, R. D.; Minteer, S. D.; Janik, M. J.; Renner, J. N.; Greenlee, L. F. Catalysts for Nitrogen Reduction to Ammonia. *Nature Catalysis*, **2018**, *1* (7), 490–500.

(6) Rohde, M.; Sippel, D.; Trncik, C.; Andrade, S. L. A.; Einsle, O. The Critical E4 State of Nitrogenase Catalysis. *Biochemistry*, **2018**, *57* (38), 5497–5504.

(7) Rutledge, H. L.; Tezcan, F. A. Electron Transfer in Nitrogenase. *Chemical Reviews*, **2020**, *120* (12), 5158–5193.

(8) Seefeldt, L. C.; Hoffman, B. M.; Peters, J. W.; Raugei, S.; Beratan, D. N.; Antony, E.; Dean, D. R. Energy Transduction in Nitrogenase. *Accounts of Chemical Research*, **2018**, *51* (9), 2179–2186.

(9) Milton, R. D.; Minteer, S. D. Nitrogenase Bioelectrochemistry for Synthesis Applications. *Accounts of Chemical Research*, **2019**, *52* (12), 3351–3360.

(10) Poudel, S.; Colman, D. R.; Fixen, K. R.; Ledbetter, R. N.; Zheng, Y.; Pence, N.; Seefeldt, L. C.; Peters, J. W.; Harwood, C. S.; Boyd, E. S. Electron Transfer to Nitrogenase in Different Genomic and Metabolic Backgrounds. *Journal of Bacteriology*, **2018**, *200* (10).

(11) Chen, J. G.; Crooks, R. M.; Seefeldt, L. C.; Bren, K. L.; Bullock, R. M.; Darensbourg, M. Y.; Holland, P. L.; Hoffman, B.; Janik, M. J.; Jones, A. K.; Kanatzidis, M. G.; King, P.; Lancaster, K. M.; Lymar, S. V; Pfromm, P.; Schneider, W. F.; Schrock, R. R. Beyond Fossil Fuel–Driven Nitrogen Transformations. *Science*, **2018**, *360* (6391), eaar6611.

(12) Gorton, L.; Meredith, M. T.; Minteer, S. D. S. D. D.; Hu, Y. J.; Lee, C. W. C.; Ribbe, M. W.; Hoffman, B. M. B. M.; Lukoyanov, D.; Yang, Z. Y.; Dean, D. R. D. R.; et al. Nitrilotriacetic Acid Degradation under Microbial Fuel Cell Environment. *Biosens. Bioelectron.*, **2010**, *5* (1), 241–248.

(13) Cadoux, C.; Milton, R. D. Recent Enzymatic Electrochemistry for Reductive Reactions. *ChemElectroChem*, **2020**, *7* (9), 1974–1986.

(14) Land, H.; Senger, M.; Berggren, G.; Stripp, S. T. Current State of [FeFe]-Hydrogenase Research: Biodiversity and Spectroscopic Investigations. *ACS Catalysis*, **2020**, *10* (13), 7069–7086.

(15) Ruth, J. C.; Milton, R. D.; Gu, W.; Spormann, A. M. Enhanced Electrosynthetic Hydrogen Evolution by Hydrogenases Embedded in a Redox-Active Hydrogel. *Chemistry - A European Journal*, **2020**, *26* (32), 7323–7329.

(16) Khanova, L. A.; Topolev, V. V.; Krishtalik, L. I. Effect of the Aqueous-Organic Solvent Structure on the Cobalticenium-Cobaltocene Redox Potential: The Redox Couple as a Basis for Determination of the Single Ion Transfer Energies. *Chemical Physics*, **2006**, *326* (1), 33–42.

(17) Tapia, C.; Milton, R. D.; Pankratova, G.; Minteer, S. D.; Åkerlund, H. E.; Leech, D.; De Lacey, A. L.; Pita, M.; Gorton, L. Wiring of Photosystem I and Hydrogenase on an Electrode for Photoelectrochemical H2 Production by Using Redox Polymers for Relatively Positive Onset Potential. *ChemElectroChem*, **2017**, *4* (1), 90–95.

(18) Kuchenreuther, J. M.; Grady-Smith, C. S.; Bingham, A. S.; George, S. J.; Cramer, S. P.; Swartz, J. R. High-Yield Expression of Heterologous [FeFe] Hydrogenases in Escherichia Coli. *PLoS ONE*, **2010**, *5* (11), e15491.

(19) Posewitz, M. C.; King, P. W.; Smolinski, S. L.; Zhang, L.; Seibert, M.; Ghirardi, M. L. Discovery of Two Novel Radical S-Adenosylmethionine Proteins Required for the Assembly of an Active [Fe] Hydrogenase. *Journal of Biological Chemistry*, **2004**, *279* (24), 25711–25720.

(20) Berggren, G.; Adamska, A.; Lambertz, C.; Simmons, T. R.; Esselborn, J.; Atta, M.; Gambarelli, S.; Mouesca, J. M.; Reijerse, E.; Lubitz, W.; Happe, T.; Artero, V.;

Fontecave, M. Biomimetic Assembly and Activation of [FeFe]-Hydrogenases. *Nature*, **2013**, *499* (7456), 66–69.

(21) Esselborn, J.; Lambertz, C.; Adamska-Venkatesh, A.; Simmons, T.; Berggren, G.; Noth, J.; Siebel, J.; Hemschemeier, A.; Artero, V.; Reijerse, E.; Fontecave, M.; Lubitz, W.; Happe, T. Spontaneous Activation of [FeFe]-Hydrogenases by an Inorganic [2Fe] Active Site Mimic. *Nature Chemical Biology*, **2013**, *9* (10), 607–609.

(22) Senger, M.; Mebs, S.; Duan, J.; Wittkamp, F.; Apfel, U. P.; Heberle, J.; Haumann, M.; Stripp, S. T. Stepwise Isotope Editing of [FeFe]-Hydrogenases Exposes Cofactor Dynamics. *Proceedings of the National Academy of Sciences of the United States of America*, **2016**, *113* (30), 8454–8459.

(23) Winkler, M.; Senger, M.; Duan, J.; Esselborn, J.; Wittkamp, F.; Hofmann, E.; Apfel, U. P.; Stripp, S. T.; Happe, T. Accumulating the Hydride State in the Catalytic Cycle of [FeFe]-Hydrogenases. *Nature Communications*, **2017**, *8* (1), 1–7.

(24) Duan, J.; Mebs, S.; Laun, K.; Wittkamp, F.; Heberle, J.; Happe, T.; Hofmann, E.; Apfel, U. P.; Winkler, M.; Senger, M.; Haumann, M.; Stripp, S. T. Geometry of the Catalytic Active Site in [FeFe]-Hydrogenase Is Determined by Hydrogen Bonding and Proton Transfer. *ACS Catalysis*, **2019**, *9* (10), 9140–9149.

(25) Felbek, C.; Hardt, S.; Papini, C.; Pramanik, D.; Artero, V.; Fontecave, M.; Fourmond, V.; Plumere, N.; Léger, C. Artificial Maturation of [FeFe] Hydrogenase in a Redox Polymer Film. *Chemical Communications*, **2021**, *accepted* (DOI: 10.1039/D0CC08168J).

(26) Goyal, A.; Marcandalli, G.; Mints, V. A.; Koper, M. T. M. Competition between CO2 Reduction and Hydrogen Evolution on a Gold Electrode under Well-Defined Mass Transport Conditions. *Journal of the American Chemical Society*, **2020**, *142* (9), 4154–4161.

(27) Ahmed, M. E.; Dey, S.; Darensbourg, M. Y.; Dey, A. Oxygen-Tolerant H2 Production by [FeFe]-H2ase Active Site Mimics Aided by Second Sphere Proton Shuttle. *Journal of the American Chemical Society*, **2018**, *140* (39), 12457–12468.

(28) Stripp, S. T.; Goldet, G.; Brandmayr, C.; Sanganas, O.; Vincent, K. A.; Haumann, M.; Armstrong, F. A.; Happe, T. How Oxygen Attacks [FeFe] Hydrogenases from Photosynthetic Organisms. *Proceedings of the National Academy of Sciences of the United States of America*, **2009**, *106* (41), 17331–17336.

(29) Sanchez, M. L. K.; Sommer, C.; Reijerse, E.; Birrell, J. A.; Lubitz, W.; Dyer, R. B. Investigating the Kinetic Competency of CrHydA1 [FeFe] Hydrogenase Intermediate States via Time-Resolved Infrared Spectroscopy. *Journal of the American Chemical Society*, **2019**, *141* (40), 16064–16070.

(30) Senger, M.; Eichmann, V.; Laun, K.; Duan, J.; Wittkamp, F.; Knör, G.; Apfel, U. P.; Happe, T.; Winkler, M.; Heberle, J.; Stripp, S. T. How [FeFe]-Hydrogenase Facilitates Bidirectional Proton Transfer. *Journal of the American Chemical Society*, **2019**, *141* (43), 17394–17403.

(31) Qiu, Y.; Ren, H.; Edwards, M. A.; Gao, R.; Barman, K.; White, H. S. Electrochemical Generation of Individual Nanobubbles Comprising H2, D2, and HD. *Langmuir*, **2020**, *36* (22), 6073–6078.